Applied Surface Science 412 (2017) 170–176

Contents lists available at ScienceDirect

Applied Surface Science

journal homepage: www.elsevier.com/locate/apsusc

Full Length Article

Rational design of Sn/SnO_2/porous carbon nanocomposites as anode materials for sodium-ion batteries

Xiaojia Li[a], Xifei Li[a,b,c,*], Linlin Fan[a], Zhuxin Yu[a], Bo Yan[a], Dongbin Xiong[a], Xiaosheng Song[a], Shiyu Li[a], Keegan R. Adair[d], Dejun Li[a,**], Xueliang Sun[d,a,*]

[a] Tianjin International Joint Research Centre of Surface Technology for Energy Storage Materials, College of Physics and Materials Science, Tianjin Normal University, Tianjin 300387, China
[b] Center for Advanced Energy Materials and Devices, Xi'an University of Technology, Xi'an 710048, China
[c] Key Laboratory of Advanced Energy Materials Chemistry (Ministry of Education), Collaborative Innovation Center of Chemical Science and Engineering, College of Chemistry, Nankai University, Tianjin 300071, China
[d] Nanomaterials and Energy Lab., Department of Mechanical and Materials Engineering, Western University, London, Ontario N6A 5B9, Canada

ARTICLE INFO

Article history:
Received 13 February 2017
Received in revised form 21 March 2017
Accepted 22 March 2017
Available online 24 March 2017

Keywords:
SnO_2
Porous carbon
Anode materials
Electrochemical performance
Sodium-ion batteries

ABSTRACT

Sodium-ion batteries (SIBs) have successfully attracted considerable attention for application in energy storage, and have been proposed as an alternative to lithium ion batteries (LIBs) due to the abundance of sodium resources and low price. Sn has been deemed as a promising anode material in SIBs which holds high theoretical specific capacity of 845 mAh g^{-1}. In this work we design nanocomposite materials consisting of porous carbon (PC) with SnO_2 and Sn (Sn/SnO_2/PC) via a facile reflux method. Served as an anode material for SIBs, the Sn/SnO_2/PC nanocomposite delivers the primary discharge and charge capacities of 1148.1 and 303.0 mAh g^{-1}, respectively. Meanwhile, it can preserve the discharge capacity approximately of 265.4 mAh g^{-1} after 50 cycles, which is much higher than those of SnO_2/PC (138.5 mAh g^{-1}) and PC (92.2 mAh g^{-1}). Furthermore, the Sn/SnO_2/PC nanocomposite possesses better cycling stability with 77.8% capacity retention compared to that of SnO_2/PC (61.88%) over 50 cycles. Obviously, the Sn/SnO_2/PC composite with excellent electrochemical performance shows the great possibility of application in SIBs.

1. Introduction

Currently, a series of environmental pollution and energy crisis have led to the urgent requirement for green and renewable energy sources. Among of them, lithium ion batteries (LIBs) with high working voltage, high energy capacity, and long cycle life conquer the portable electronic markets, and have become the primary choice of energy storage in electric vehicles (EVs) and hybrid electric vehicles (HEVs). However, the global lithium resources will not be effective in meeting the huge demands of LIBs, which will further inflate the prices of materials associated with lithium, increase the cost of the batteries and eventually hinder the development of new energy industry. Therefore, it is significant to explore an alternative cost-effective energy storage technology.

The development of sodium ion batteries (SIBs) can be traced back to the late 1980s along with the emergence of LIBs [1]. Currently, much effort has been devoted to researching SIB energy storage system. Remarkably, SIBs possess three obvious advantages over LIBs: (i) raw material is abundant with low cost and wide distribution; (ii) sodium precursors are more environmentally friendly compared to lithium [2]; (iii) SIBs reveal relatively stable electrochemical performance with high safety performance. However, some intrinsic drawbacks still exist in SIBs, for instance, the relative atomic mass of sodium is much higher than that of lithium, leading to relatively low theoretical specific capacity. Moreover, the radius of Na^+ is larger than that of Li^+, which results in the difficulties of electrode reaction kinetics. Unfortunately, the anode materials of typical graphitic carbons utilized in LIBs can barely intercalate Na^+ ions. Undoubtedly, one of the most important challenges in the research of SIBs is the design of suitable electrode materials.

At present, a large number of anode materials have been proposed for SIBs, such as Sn [2–6], Sb [2,5,7], SnS [5,7], SnS_2 [3], SnO_2 [3,4,6,8–10], TiO_2 [10], MoS_2 [1]. Of which, SnO_2 has been extensively studied due to its low cost, large reserves, high theoretical capacity, and good safety. Previously, researchers have designed

* Corresponding authors at: Tianjin International Joint Research Centre of Surface Technology for Energy Storage Materials, College of Physics and Materials Science, Tianjin Normal University, Tianjin 300387, China
** Corresponding author.
E-mail addresses: xfli2011@hotmail.com (X. Li), dejunli@mail.tjnu.edu.cn (D. Li), xsun9@uwo.ca (X. Sun).

http://dx.doi.org/10.1016/j.apsusc.2017.03.203
0169-4332/

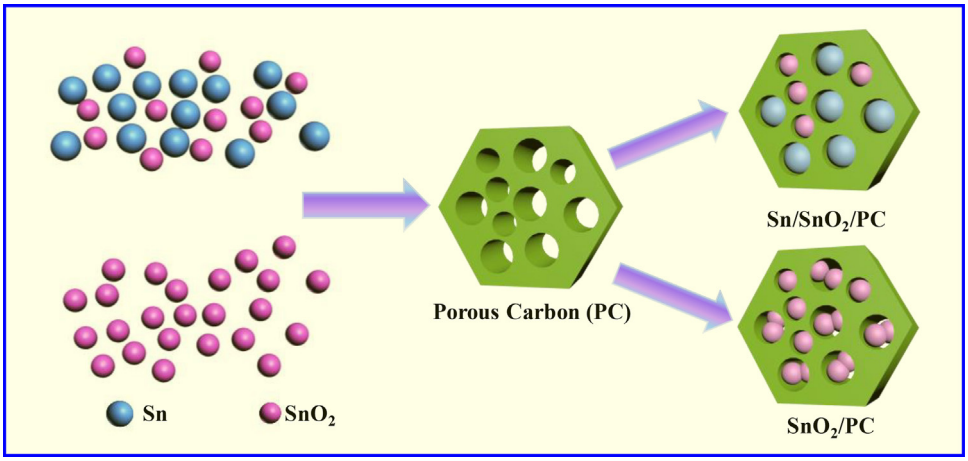

Scheme 1. Schematic illustration for the synthesis process of $Sn/SnO_2/PC$ and SnO_2/PC.

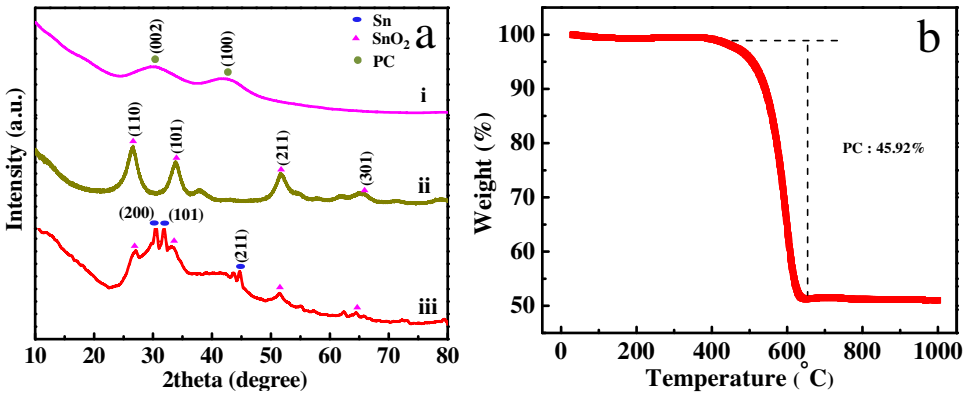

Fig. 1. (a) XRD patterns of (i) pristine PC, (ii) SnO_2/PC, and (iii) $Sn/SnO_2/PC$; (b) TGA curve of $Sn/SnO_2/PC$.

various SnO_2-based anode materials for SIBs, such as SnO_2@RGO [9] and SnO_2@CNT [4]. For example, carbon coated SnO_2 materials synthesized via a hydrothermal process revealed obvious capacity fade and only maintained 100 mAh g^{-1} after 50 cycles for SIBs [11]. Via an in-situ hydrothermal method, the SnO_2/nitrogen-doped graphene nanohybrids (SnO_2/NG) delivered reversible capacity of 180 mAh g^{-1} in the 50th cycle at a current density of 20 mA g^{-1} for SIBs [10]. More interestingly, Sn-based materials hold higher theoretical reversible capacity of 847 mAh g^{-1} [4], and numerous means have been reported to compose Sn-based nanocomposites [12–14]. One CVD method was adopted to synthesize Sn@C nanospheres as SIBs anode materials [15]. Unfortunately, its specific capacity dropped to 52 mAh g^{-1} after 50 cycles at a current density of 40 mA g^{-1} due to large volume expansion. To address the obvious capacity fading, the $Sn/SnO_2/C$ composites with well-designed structure were fabricated where Sn and SnO_2 nanoparticles were encapsulated in a carbon matrix. As a result, the composites displayed superior cycling stability and rate capability compared to SnO_2/C and Sn/C. The enhanced sodium storage performance of $Sn/SnO_2/C$ anode is attributed to the synergistic effect provided by Sn, SnO_2 and unique core-shell structure. Meanwhile, the carbon matrix could act as a buffer to accommodate the volume change effect [14]. In addition, one similar structure of sandwich-like CNTs@SnO_2/SnO/Sn materials was reported to deliver superior electrochemical performance as anode materials for LIBs [4]. The superior electrochemical performance of Sn/SnO_2 nanocomposites suggests that it may be a promising anode material for SIBs. However, the extreme volume expansion of Sn needs to be accommodated. As far as we know, both graphene and carbon nanotubes are excellent matrices to overcome the aforementioned challenges, while high cost restricts their practical application. By comparison, porous carbon (PC) is a preferable choice to be the assist of the Sn/SnO_2 anode which can attribute to its outstanding buffering effect, higher electronic conductivity [6], and largely increase of the active surface area [16–18].

In this study, a $Sn/SnO_2/PC$ nanocomposite was successfully synthesized through a facile reflux method. Meanwhile, PC was obtained using pine cones as a low cost carbon source. It is believed that the PC matrix may further increase electrochemical performance of the Sn/SnO_2 anode materials for SIBs.

2. Experiments

2.1. Synthesis of PC

PC was synthesized by nature pineal gland. Firstly, the pineal gland (pine) were cleaned by deionized water and dilute hydrochloric acid under magnetic stirring for 3 h, and subsequently dried in the oven at 80 °C for two days. Afterwards, the dried pineal gland was put in the muffle furnace to pre-carbonize at 350 °C for 4 h in air at the rate of 4 °C min^{-1}. Next, 1.0 g carbon sample and 5.0 g KOH solid were dissolved in deionized water with ultrasonic stirring for 24 h. Subsequently, the obtained sample was heated in annealing furnace tube at 750 °C for 1.5 h in Ar environment. Finally, the post-annealing product was put into hydrochloric acid to remove the residual KOH. PC was obtained via freeze – drying.

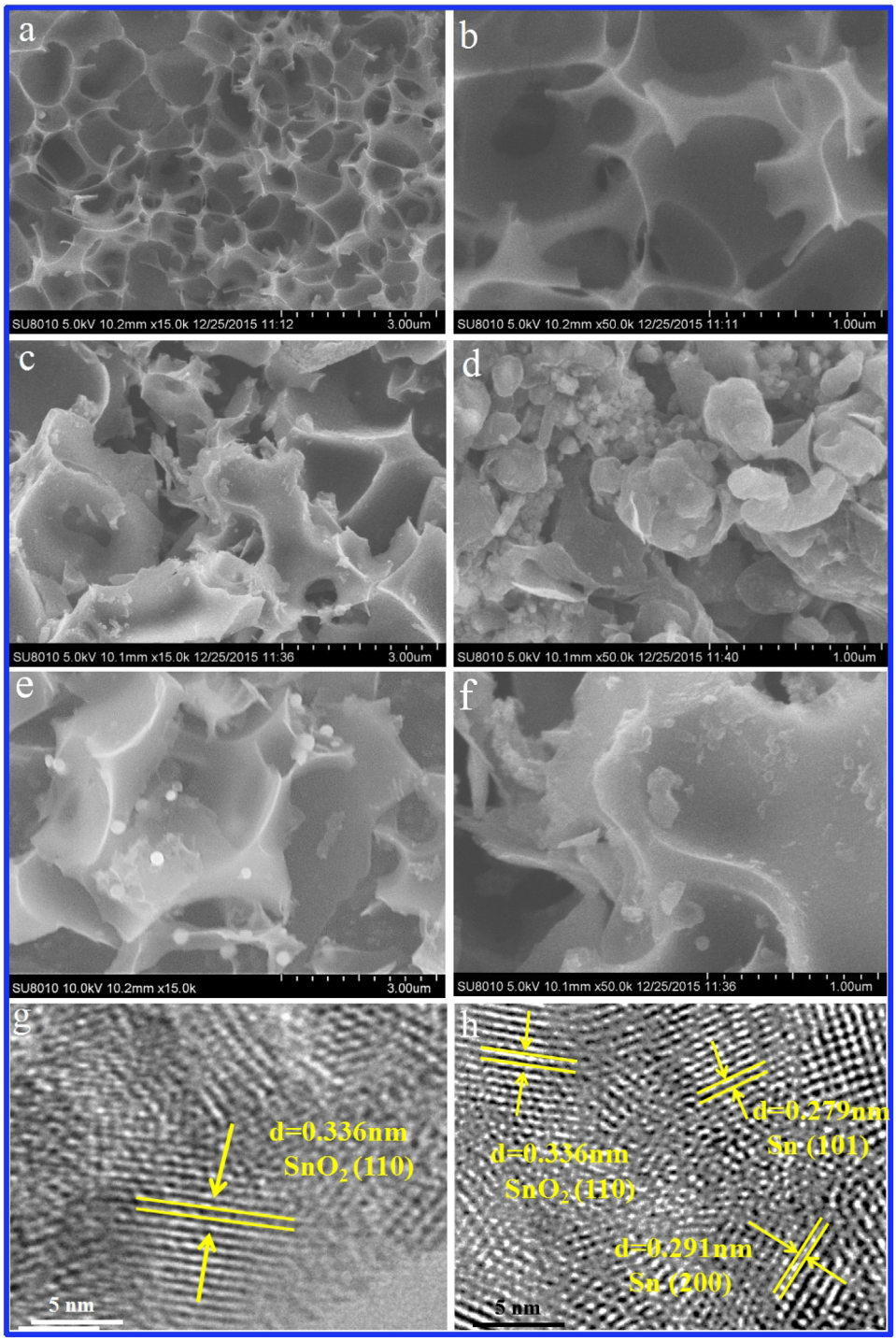

Fig. 2. Typical SEM images of (a, b) PC, (c, d) SnO_2/PC, (e, f) Sn/SnO_2/PC; HRTEM images of (g) SnO_2/PC, (h) Sn/SnO_2/PC.

2.2. Synthesis of Sn/SnO_2/PC nanocomposites

The synthesis processes of Sn/SnO_2/PC and SnO_2/PC were illustrated in Scheme 1. In general, 81 mg $SnCl_2{\cdot}2H_2O$ (Tianjin Fengchuan Chemical Reagent Science And Technology Co., Ltd. ≥ 98.0%) was firstly dispersed in 50 mL ethanol (Tianjin Jiangtian Chemical Technology Co., Ltd.) under vigorous magnetic stirring for 0.5 h. At the same time, 38 mg PC was dispersed in 50 mL ethylene glycol by ultrasonication for 0.5 h and placed in a 100 mL three-neck flask, followed by heating at 100 °C in an oil bath. Afterwards, the $SnCl_2$-ethanol solution was transferred to the PC-ethylene glycol solution dropwise and refluxed at 100 °C for 12 h. The resultant product was separated and cleaned with ethanol and deionized water for several times. The product was dried at 80 °C for 10 h in the oven. Ultimately, the Sn/SnO_2/PC nanocomposites were obtained via calcination in an argon atmosphere at 500 °C for 3 h in the tube furnace. The preparation process of SnO_2/PC nanocomposites was similar to that of the Sn/SnO_2/PC, but 50 mL ethylene glycol was replaced by 50 mL deionized water. The pristine PC was obtained by treating PC using the same method without the introduction of $SnCl_2{\cdot}2H_2O$.

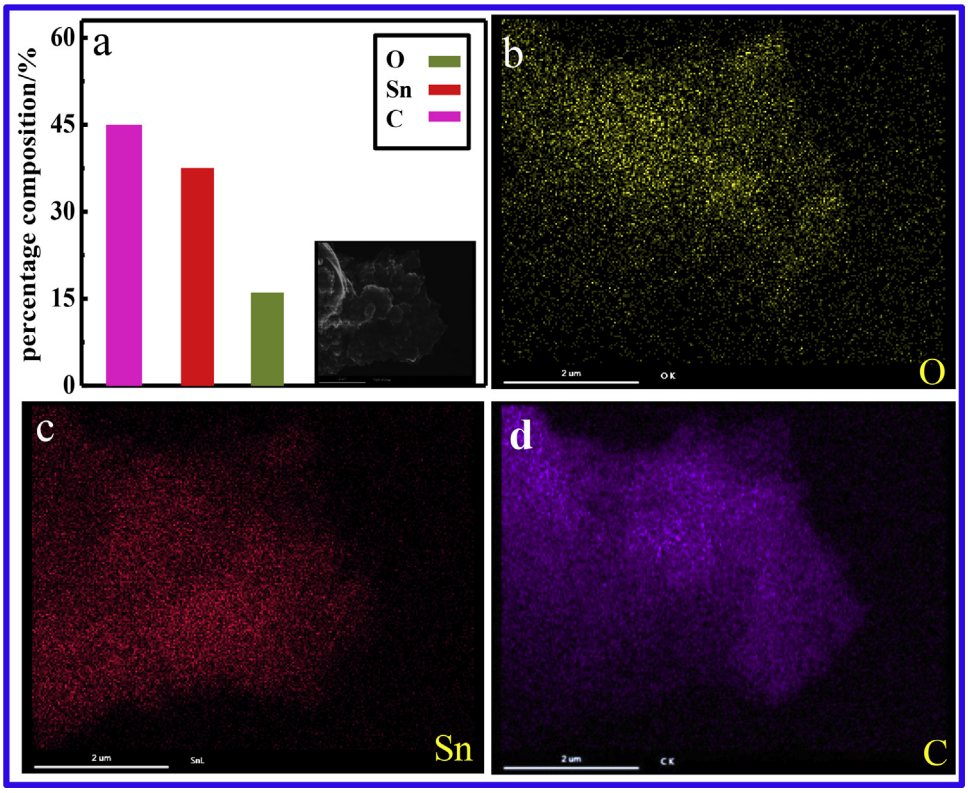

Fig. 3. (a) Element proportional and SEM image of $Sn/SnO_2/PC$; The elemental mapping of (b) O, (c) Sn, and (d) C of $Sn/SnO_2/PC$.

2.3. Physical characterization

The as-prepared materials were characterized by X-ray diffraction (XRD, DX-2700) with Cu-K_α radiation ($\lambda = 1.5405$ Å), and the data was collected between scattering angles (2θ) of 5–80° at a scanning rate of 8° min^{-1}. The PC contents in the composites were confirmed via thermogravimetric analysis (TGA, Pyris Diamond6000 TG/DTA, PerkinElmer Co, America). The morphologies and structure of products were characterized with scanning electron microscopy (SEM, SU8010, Hitachi) and high-resolution transmission electron microscopy (HRTEM, JEOL JEM-3000F). The energy dispersive spectroscopy (EDS) was recorded at 20 kV.

2.4. Electrochemical characterizations

The working electrodes were prepared by casting the slurry (70 wt% active material, 20 wt% conductive carbon black, and 10 wt% polyvinylidene fluoride (PVDF) in an *N*-methyl-2-pyrrolidene (NMP) solvent on copper foil. Afterwards, the working electrodes were dried overnight at 80 °C under vacuum. The electrodes were punched into 12 mm disks in diameter. 10 pieces of copper foils with the size of 12 mm in diameter were weighed using a high resolution balance (0.01 mg), and the average weight of each copper foil was calculated to be 9.8 mg. Then the mass of active material was calculated using a conventional algorithm, namely, the electrode weight of $Sn/SnO_2/PC$ nanocomposites subtracts the average weight of the copper foils, and the 70% of the calculated result is the mass of $Sn/SnO_2/PC$. Based on this value, the specific capacity of the $Sn/SnO_2/PC$ nanocomposites may be calculated. In the argon-filled glove box, the coin cells were assembled with oxygen and moisture levels less than 0.1 ppm. A sodium sheet was used as the counter electrode and reference electrode. A solution of 1 M $NaClO_4$ dissolved in ethylene carbonate (EC) and propylene carbonate (PC) at a volume ratio of 2:1 accompany with the addition of 10 vol% fluoroethylene carbonate (FEC) was used for the electrolyte. 2032 type coin cells were utilized to evaluate the electrochemical performance of the as-prepared anode materials. Cycling performance and rate capability were galvanostatically tested in the voltage range of 0.01–3.0 V (vs. Na/Na^+) at various current densities by a Land batteries test system (LANHE CT2001A). Electrochemical impedance spectroscopy (EIS) was carried out at an amplitude of 5 mV over the frequency range from 100 kHz to 0.01 Hz. Cyclic voltammetry (CV) was tested at the scanning rate of 0.1 mV s^{-1} in the voltage range of 0.01–3.0 V. Both of them were carried out using a Princeton Applied Research VersaSTAT4 electrochemical workstation.

3. Results and discussion

Fig. 1a displays the X-ray diffraction (XRD) patterns of as-prepared samples. It is clear that the pristine PC displays (002) and (100) diffraction peaks. The diffraction peaks of SnO_2/PC material centered at $2\theta = 26.58°$, 33.87°, 51.77°, and 65.96° correspond to (110), (101), (211), and (301) crystal planes of SnO_2 (JCPDS No. 71-0652), respectively, which are extremely similar to those of previous reports [1,6,19–22]. In addition to SnO_2 diffraction peaks, $Sn/SnO_2/PC$ reveals the characteristic peaks of Sn. Two sharp diffraction peaks located at 30.63°, 32.01° and a weak peak centered at 44.89° can be seen clearly, which are interrelated to (200), (101), and (211) crystal planes of Sn (JCPDS No. 78-0210), respectively. These observations suggest the successful incorporation of Sn and SnO_2 into PC material. The thermogravimetric analysis (TGA) of $Sn/SnO_2/PC$ was measured in air. As shown in Fig. 1b, one can see an obvious weight loss between 350 °C and 650 °C, which could attribute to the decrease of PC. Therefore, it is estimated that the loading of PC is about 46 wt%.

Fig. 2a and b shows SEM images of the PC. In Fig. 2a, the large, porous cavities can be observed on the surface of the material that

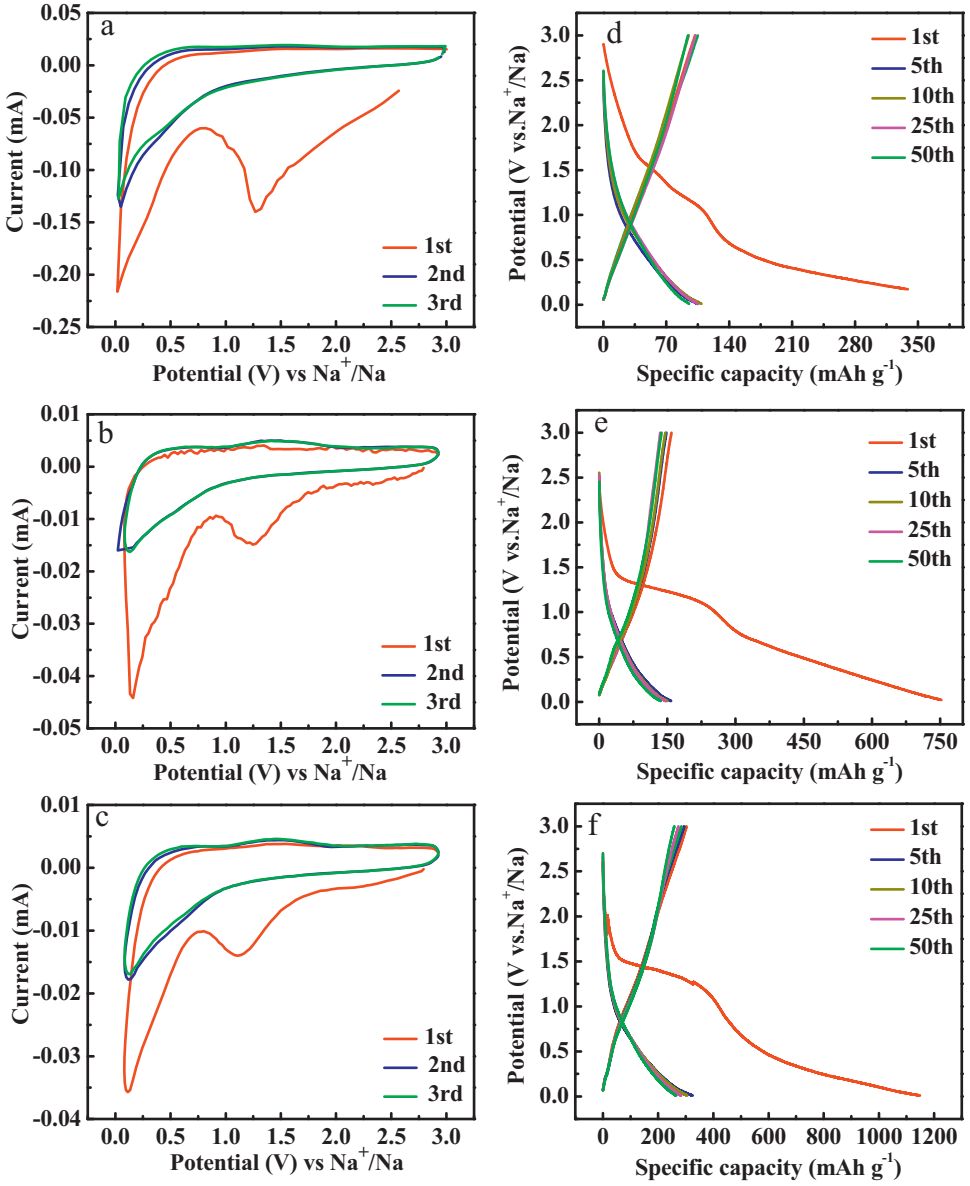

Fig. 4. The CV curves of (a) pristine PC, (b) SnO_2/PC, and (c) Sn/SnO_2/PC at a scan rate of 0.1 mV s^{-1} in the voltage range of 0.01–3.0 V; The discharge/charge profiles of (d) pristine PC, (e) SnO_2/PC, and (f) Sn/SnO_2/PC in the 1st, 5th, 10th, 25th, and 50th cycles.

proves the formation of PC. At high magnification (see Fig. 2b), it is apparent that the pore size of PC is around 500 nm. The morphologies of SnO_2/PC are displayed in Fig. 2c and d. It can be observed that SnO_2 particles are evenly dispersed in the PC. Fig. 2e and f suggest that Sn and SnO_2 particles are scattered inside of PC. Fig. 2f further reveals that both Sn and SnO_2 are well-distributed with the PC material. Moreover, the successive lattice fringe of SnO_2/PC is distinctly viewed in Fig. 2g, displaying that the SnO_2 particles are crystallized. The lattice spacing of 0.336 nm corresponds to the (110) plane of SnO_2. Additionally, the lattice image in Fig. 2h reveals lattice spacings of 0.279 and 0.291 nm, which correspond to the (101) and (200) crystal planes of Sn, respectively. These results are in good agreement with the XRD analysis and further confirm that the Sn/SnO_2/PC is successfully fabricated via our proposed method. As shown in Fig. 3, the elements of Sn/SnO_2/PC are confirmed by EDS, which certifies the uniform distribution of O, Sn, and C in the nanocomposites without other impurities.

Cyclic voltammetry (CV) of PC, SnO_2/PC and Sn/SnO_2/PC anodes was executed to examine the electrochemical behavior of sodium storage at the scanning rate of 0.1 mV s^{-1} in the voltage range of 0.01–3.0 V. Fig. 4a displays the typical electrochemical behavior of pristine PC for SIBs. In the first discharge process, there is a peak centered at 1.25 V due to the formation of solid electrolyte interphase (SEI). In comparison with PC, the CV curves of SnO_2/PC and Sn/SnO_2/PC anodes are similar, as shown in Fig. 4b and c. Clearly, there are different peaks in the first cycle compared to the succeeding cycles during the Na^+ insertion/extraction. The cathodic peaks of SnO_2/PC and Sn/SnO_2/PC appear at around 1.25 V, which can be attributed to the SEI layer formation as well as the electrochemical reaction of SnO_2 with Na forming the Sn and Na_2O by Eq. (1) [24]. Nevertheless, in the following scans, the cathodic peaks disappear due to the irreversible reactions. Another reductive peak positioned at around 0.5 V is assigned to the formation of $Na_{3.75}Sn$ with adsorption of Na^+ on the porous carbon by Eqs. (2) and (3) [22]. The peak position was not obvious, and it might be due to high content of porous carbon in the nanocomposites. Meanwhile, it can be seen that the CV profiles in the second and third cycles almost overlap, indicating good cycle reversibility. Furthermore,

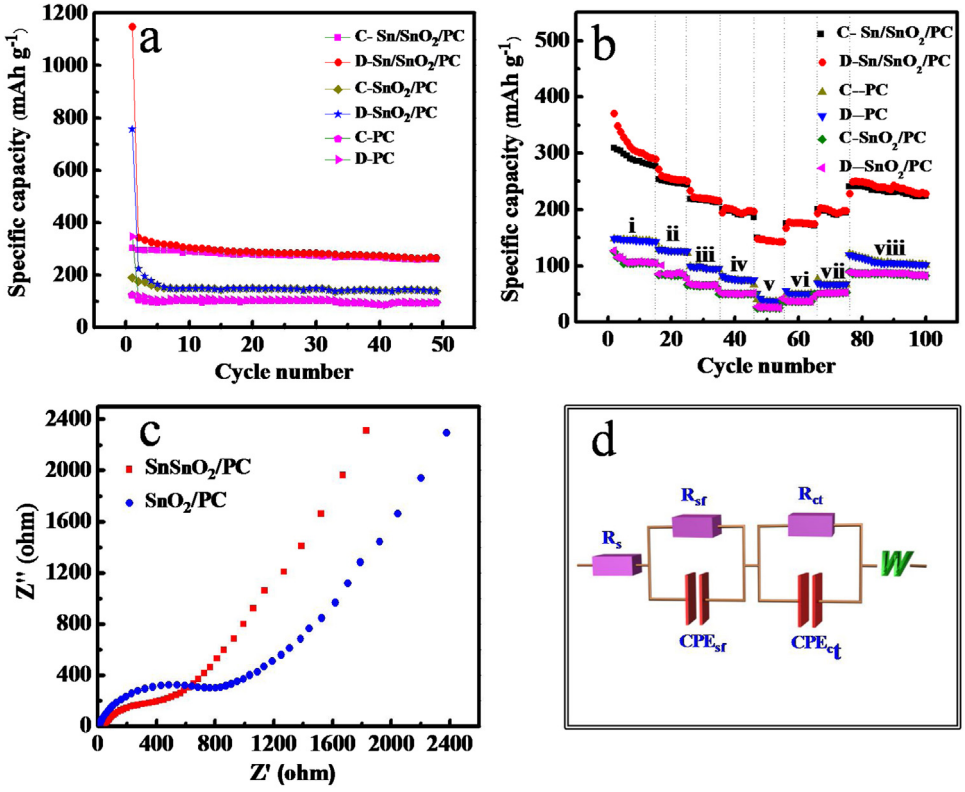

Fig. 5. (a) Cycling performances of pristine PC, SnO_2/PC, and Sn/SnO_2/PC; (b) Rate performances of pristine PC, SnO_2/PC, and Sn/SnO_2/PC at different current density ranging from 25 mA g^{-1} to 400 mA g^{-1}; (c) The electrochemical impedance spectroscopy of SnO_2/PC and Sn/SnO_2/PC in the 5th cycle; (d) The equivalent circuit used to simulate EIS curves.

during charging process, the anodic peaks are recognized clearly around at 0.5 V and 1.5 V, which indicate the phase transition of Na-Sn alloying to Sn. Meanwhile, it can be seen that the second and third cycles almost overlap, indicating good cycle reversibility. The electrochemical processes can be described as follows [22]:

$$SnO_2 + 4Na \rightarrow Sn + 2Na_2O \quad (1)$$

$$Sn + 3.75Na \leftrightarrow Na_{3.75}Sn(Na_{15}Sn_4) \quad (2)$$

$$xC + Na^+ + e^- \leftrightarrow NaC_x \quad (3)$$

As shown in Fig. 4d–f, the typical voltage profiles of pristine PC, SnO_2/PC, and Sn/SnO_2/PC were compared in a voltage range from 0.01 to 3.0 V at a current density of 50 mA g^{-1}. In Fig. 4d, the PC displays a low reversible capacity of 94.2 mAh g^{-1}. In Fig. 4e and f, both of SnO_2/PC and Sn/SnO_2/PC reveal the analogous tendency of a stable plateau at 1.25 V which could be attributed to the SEI formation [5,19,25] and the irreversible transformation during the initial discharge process. The first discharge and charge capacities of SnO_2/PC are observed to be around 756.8 and 189.5 mAh g^{-1}, respectively, while the initial discharge and charge capacities of Sn/SnO_2/PC increase to 1148.1 and 303.0 mAh g^{-1}, respectively. However, the large capacity loss in the initial cycle is likely attributed to the irreversible reaction as described in Eq. (1), the decomposition of electrolyte and inevitable formation of the SEI layer. As well known, Sn has been deemed as a great anode material in SIBs which holds high theoretical specific capacity of 845 mAh g^{-1} [4], and SnO_2 reveals the theoretical capacity of 667 mAh g^{-1} [1]. But, the theoretical capacity of PC may not be calculated due to its variety of nanostructure. As a result, the theoretical capacity of Sn/SnO_2/PC nanocomposites may not be estimated accurately. As shown in Fig. 5a, after 50 cycles, the energy capacity of Sn/SnO_2/PC is seen to be higher than that of SnO_2/PC. The enhanced Na-storage capacity of the Sn/SnO_2/PC electrode may be due to the dispersion of nano-sized Sn particles [26], which have a higher theoretical reversible capacity than SnO_2.

The cycling performances of the pristine PC, SnO_2/PC and Sn/SnO_2/PC anodes were tested at room temperature at a current density of 50 mA g^{-1} in the voltage range of 0.01–3.0 V (see Fig. 5a). It is apparent that the reversible capacity of pristine PC only maintains 92.2 mAh g^{-1} after 50 cycles. Fortunately, the introduction of SnO_2 presents an enhanced discharge capacity of 138.5 mAh g^{-1} in the 50th cycle, and the capacity retention is around 62% compared to the second reversible capacity of 223.8 mAh g^{-1}. As seen clearly, the second reversible capacity of Sn/SnO_2/PC anode is around 341.5 mAh g^{-1}, and it can deliver good reversible capacity of 265.4 mAh g^{-1} after 50 cycles with higher capacity retention of 77.8%. Fig. 5b compares the rate capability of PC, SnO_2/PC and Sn/SnO_2/PC at various current densities varying from 25 to 400 mA g^{-1}. It is noted that PC and SnO_2/PC electrodes exhibit lower rate capabilities at higher current densities. Significantly, the Sn/SnO_2/PC works well at all current densities. In Fig. 5b, one can see that the discharge capacities of Sn/SnO_2/PC are 311.8, 253.7, 221.5, 195.4, and 146.3 mAh g^{-1} at current densities of 25, 50, 100, 200, and 400 mA g^{-1}, respectively. Moreover, it maintains high reversible capacity of 230 mAh g^{-1} after the current density decreases back to 50 mA g^{-1} in the 81th cycle, showing better rate capability than that of PC and SnO_2/PC.

Electrochemical impedance spectroscopy (EIS) was employed to understand the kinetics of sodium storage at the charge condition (around 1.5 V), as described in Fig. 5c. The Nyquist plots are composed of two parts with a hemisphere-like shape and inclined line. One can observe that the diameter of the intermediate frequency region of SnO_2/PC is bigger than that of the Sn/SnO_2/PC, illustrating that Sn/SnO_2/PC has smaller charge transfer impedance [27], which is beneficial for Na^+ extraction/insertion [3,28]. The equivalent circuit in Fig. 5d was utilized to fit the EIS curves. R_s signifies ohmic

electrolyte resistance, R_{sf} delegates surface SEI film resistance and R_{ct} denotes the resistance of charge transfer. In addition, CPE_{sf} and CPE_{ct} are related to constant phase elements of the surface film and double layer capacitance, respectively. W represents Warburg impedance for solid state diffusion [23]. According to the equivalent circuit, the R_{ct} of the Sn/SnO_2/PC electrode is calculated to be 378.2 Ω, which is much smaller than that of the SnO_2/PC electrode (787.3 Ω), further confirming the superior electrochemical performance of Sn/SnO_2/PC over SnO_2/PC.

It is evident that the Sn/SnO_2/PC anode exhibits better cycling performance and rate capability than the pristine PC and SnO_2/PC. During the initial discharge process, SnO_2 is reduced into Sn and Na_2O as shown in Eq. (1). Subsequently, Sn may alloy with Na as suggested by Eq. (2) resulting in problematic volume expansion. In this study, for the first time, the Sn/SnO_2/PC nanocomposites were synthetized successfully via a facile reflux method for SIBs. The nanocomposites hold unique structure. Both Sn and SnO_2 were designed to uniformly distribute into PC with high surface area and good electrical conductivity. As shown in Scheme 1, PC in the composite plays a vital role in improving the electrochemical performance due to its ability to disperse the particles uniformly, providing contact for electrical conductivity and buffering the volume expansion of Sn and SnO_2 in the sodiation/desodiation processes. Meanwhile, the synergistic effect of Sn and SnO_2 also contributes to enhancing electrochemical performance [14]. As a result, as anodes for SIBs, the Sn/SnO_2/PC nanocomposites can deliver high discharge capacity of 265.4 mAh g^{-1} after 50 cycles, which is much higher than those of SnO_2/PC (138.5 mAh g^{-1}) and PC (92.2 mAh g^{-1}). Therefore, the novel nanocomposites we designed reveal promising as anodes for SIBs.

4. Conclusions

In summary, the SnO_2/PC and Sn/SnO_2/PC nanocomposites were successfully obtained via a facile reflux method. In comparison with SnO_2/PC and PC, the cycling performance of Sn/SnO_2/PC has been substantially improved, maintaining a discharge capacity of 265.4 mAh g^{-1} after 50 cycles. The Sn/SnO_2/PC composite outperforms the other materials in rate capabilities, energy capacity and cycling stability at a variety of current densities. Especially, it can achieve a discharge capacity of 146.3 mAh g^{-1} at 400 mA g^{-1}. The better performance of Sn/SnO_2/PC composite benefits from the enhanced conductivity of PC and Sn. Moreover, PC can effectively buffer the volume expansion/shrinkage upon cycling. Thus, the Sn/SnO_2/PC material is a prospective anode material for high performance SIBs.

Acknowledgments

This research was supported by the National Natural Science Foundation of China (51572194 and 51672189), Academic Innovation Funding of Tianjin Normal University(52XC1404), and the program of Thousand Youth Talents in Tianjin of China, XS thanks support from the Natural Science and Engineering Research Council of Canada and the Canada Research Chair Program.

References

[1] L. Fan, X. Li, B. Yan, J. Feng, D. Xiong, D. Li, L. Gu, Y. Wen, S. Lawes, X. Sun, Controlled SnO_2 crystallinity effectively dominating sodium storage performance, Adv. Energy Mater. (2016) 1502057.
[2] Y. Cheng, J. Huang, R. Li, Z. Xu, L. Cao, H. Ouyang, J. Li, H. Qi, C. Wang, Enhanced cycling performances of hollow Sn compared to solid Sn in Na-ion battery, Electrochim. Acta 180 (2015) 227–233.
[3] Y. Zhang, J. Xie, S. Zhang, P. Zhu, G. Cao, X. Zhao, Ultrafine tin oxide on reduced graphene oxide as high-performance anode for sodium-ion batteries, Electrochim. Acta 151 (2015) 8–15.
[4] J. Zhang, Z. Ma, W. Jiang, Y. Zou, Y. Wang, C. Lu, Sandwich-like CNTs@SnO_2/SnO/Sn anodes on three-dimensional Ni foam substrate for lithium ion batteries, J. Electroanal. Chem. 767 (2016) 49–55.
[5] X. Xie, K. Kretschmer, J. Zhang, B. Sun, D. Su, G. Wang, Sn@CNT nanopillars grown perpendicularly on carbon paper: a novel free-standing anode for sodium ion batteries, Nano Energy 13 (2015) 208–217.
[6] P. Wu, N. Du, H. Zhang, J. Yu, Y. Qi, D. Yang, Carbon-coated SnO_2 nanotubes: template-engaged synthesis and their application in lithium-ion batteries, Nanoscale 3 (2011) 746–750.
[7] M. Gu, A. Kushima, Y. Shao, J.G. Zhang, J. Liu, N.D. Browning, J. Li, C. Wang, Probing the failure mechanism of SnO_2 nanowires for sodium-ion batteries, Nano Lett. 13 (2013) 5203–5211.
[8] Y. Cheng, J. Huang, J. Li, Z. Xu, L. Cao, H. Ouyang, J. Yan, H. Qi, SnO_2/super P nanocomposites as anode materials for Na-ion batteries with enhanced electrochemical performance, J. Alloys Compd. 658 (2016) 234–240.
[9] Z. Du, X. Yin, M. Zhang, Q. Hao, Y. Wang, T. Wang, In situ synthesis of SnO_2/graphene nanocomposite and their application as anode material for lithium ion battery, Mater. Lett. 64 (2010) 2076–2079.
[10] X. Xie, D. Su, J. Zhang, S. Chen, A.K. Mondal, G. Wang, A comparative investigation on the effects of nitrogen-doping into graphene on enhancing the electrochemical performance of SnO_2/graphene for sodium-ion batteries, Nanoscale 7 (2015) 3164–3172.
[11] Y. Liu, X. Fang, M. Ge, J. Rong, C. Shen, A. Zhang, H.A. Enaya, C. Zhou, SnO_2 coated carbon cloth with surface modification as Na-ion battery anode, Nano Energy 16 (2015) 399–407.
[12] Z. Du, S. Zhang, T. Jiang, Z. Bai, Preparation and characterization of three-dimensional tin thin-film anode with good cycle performance, Electrochim. Acta 55 (2010) 3537–3541.
[13] K. Zhuo, M.-G. Jeong, C.-H. Chung, Highly porous dendritic Ni–Sn anodes for lithium-ion batteries, J. Power Sources 244 (2013) 601–605.
[14] Y. Cheng, J. Huang, J. Li, Z. Xu, L. Cao, H. Qi, Synergistic effect of the core-shell structured Sn/SnO_2/C ternary anode system with the improved sodium storage performance, J. Power Sources 324 (2016) 447–454.
[15] W. Chen, D. Deng, Carbonized common filter paper decorated with Sn@C nanospheres as additive-free electrodes for sodium-ion batteries, Carbon 87 (2015) 70–77.
[16] J.-C. Kim, D.-W. Kim, Synthesis of multiphase SnSb nanoparticles-on-SnO_2/Sn/C nanofibers for use in Li and Na ion battery electrodes, Electrochem. Commun. 46 (2014) 124–127.
[17] I. Meschini, F. Nobili, M. Mancini, R. Marassi, R. Tossici, A. Savoini, M.L. Focarete, F. Croce, High-performance Sn@carbon nanocomposite anode for lithium batteries, J. Power Sources 226 (2013) 241–248.
[18] H. Ming, J. Ming, W.-J. Kwak, W. Yang, Q. Zhou, J. Zheng, Y.-K. Sun, Fluorine-doped porous carbon-decorated Fe_3O_4-FeF_2 composite versus $LiNi_{0.5}Mn_{1.5}O_4$ towards a full battery with robust capability, Electrochim. Acta 169 (2015) 291–299.
[19] H. Song, X. Li, Y. Cui, D. Xiong, Y. Wang, J. Zeng, L. Dong, D. Li, X. Sun, Controllable lithium storage performance of tin oxide anodes with various particle sizes, Int. J. Hydrogen Energy 40 (2015) 14314–14321.
[20] Y. Wang, D. Su, C. Wang, G. Wang, SnO_2@MWCNT nanocomposite as a high capacity anode material for sodium-ion batteries, Electrochem. Commun. 29 (2013) 8–11.
[21] P. Lian, S. Liang, X. Zhu, W. Yang, H. Wang, A novel Fe_3O_4-SnO_2-graphene ternary nanocomposite as an anode material for lithium-ion batteries, Electrochim. Acta 58 (2011) 81–88.
[22] Y.-X. Wang, Y.-G. Lim, M.-S. Park, S.-L. Chou, J.H. Kim, H.-K. Liu, S.-X. Dou, Y.-J. Kim, Ultrafine SnO_2 nanoparticle loading onto reduced graphene oxide as anodes for sodium-ion batteries with superior rate and cycling performances, J. Mater. Chem. A 2 (2014) 529–534.
[23] L. Fan, X. Li, Y. Cui, H. Xu, X. Zhang, D. Xiong, B. Yan, Y. Wang, D. Li, Tin oxide/graphene aerogel nanocomposites building superior rate capability for lithium ion batteries, Electrochim. Acta 176 (2015) 610–619.
[24] X. Sun, X. Wang, L. Qiao, D. Hu, N. Feng, X. Li, Y. Liu, D. He, Electrochemical behaviors of porous SnO_2-Sn/C composites derived from pyrolysis of SnO_2/poly(vinylidene fluoride), Electrochim. Acta 66 (2012) 204–209.
[25] L.Z. Fan, Y.S. Hu, J. Maier, P. Adelhelm, B. Smarsly, M. Antonietti, High electroactivity of polyaniline in supercapacitors by using a hierarchically porous carbon monolith as a support, Adv. Funct. Mater. 17 (2007) 3083–3087.
[26] S. Komaba, Y. Matsuura, T. Ishikawa, N. Yabuuchi, W. Murata, S. Kuze, Redox reaction of Sn-polyacrylate electrodes in aprotic Na cell, Electrochem. Commun. 21 (2012) 65–68.
[27] N. Li, H. Song, H. Cui, C. Wang, Sn@graphene grown on vertically aligned graphene for high-capacity, high-rate, and long-life lithium storage, Nano Energy 3 (2014) 102–112.
[28] L. Wu, X. Hu, J. Qian, F. Pei, F. Wu, R. Mao, X. Ai, H. Yang, Y. Cao, A Sn-SnS-C nanocomposite as anode host materials for Na-ion batteries, J. Mater. Chem. A 1 (2013) 7181.